# Magnetic flux coordinates for analytic high-beta tokamak equilibria with flow

**Atsushi Ito**[1] **and Noriyoshi Nakajima**[2]

[1] National Institute for Fusion Science, National Institutes of Natural Sciences, 322-6 Oroshi-cho, Toki, Gifu 509-5292 Japan

[2] Rokkasho Research Center, National Institute for Fusion Science, National Institutes of Natural Sciences, 2-166 Omotedate, Obuchi, Rokkasho, Kamikita, Aomori 039-3212 Japan

**Abstract.** Magnetic flux coordinates are constructed from an analytic solution (Ito A and Nakajima N 2009 *Plasma Phys. Control. Fusion* **51** 035007) for the reduced magnetohydrodynamics (MHD) equilibrium equations for high-beta tokamaks in the presence of poloidal and toroidal flows comparable to the poloidal sound velocity. The analytic solution indicates non-circular magnetic flux surfaces and transition between sub- and super-sonic poloidal flows. The magnetic flux coordinates for such non-circular magnetic flux surfaces are obtained for stability analysis. The flux coordinates are numerically obtained from the high order polynomial equations for the relation with the geometrical coordinates. As applications, pressure profiles in the poloidal direction on each flux surface, which become non-constant due to flow, and the flux average of the pressure are obtained. The transitions of the pressure profiles and the flux average of the pressure between sub- and super-sonic poloidal flows are discussed in relation with the radial force balance. The flux coordinates are also obtained analytically by expanding the coordinate relations with respect to the inverse aspect ratio.

## 1. Introduction

Axisymmetric, static magnetohydrodynamics (MHD) equilibrium is described by the Grad-Shafranov (GS) equation. Usual solutions compose nested magnetic flux surfaces, and the pressure is constant on each magnetic flux surface. For high-beta tokamaks, the magnetic flux surfaces are non-circular and the magnetic axis is shifted outwards in the major radius of a torus due to the Shafranov shift. To study the stability of such equilibrium, magnetic flux coordinates constructed from the solutions of the GS equation are exploited [1, 2, 3]. An analytic representation of the flux coordinate system was derived [4] from an analytic solution for the first order with respect to the inverse aspect ratio of a torus of the GS equation for the high-beta tokamaks [5, 6]. Such a flux coordinate system is favorable for analyzing the stability in the equilibria with large pressure gradient.

For axisymmetric MHD equilibrium with flow, the governing equation is called the generalized GS equation [7, 8]. The pressure $p$ is no longer constant on each magnetic flux surface $\psi = const.$ in the presence of flow,

$$p \neq p(\psi), \tag{1}$$

though equilibrium is still determined with free functions of the magnetic flux. The pressure is non-constant on each magnetic flux surface even for purely toroidal flow. The analytic solution for purely toroidal flow is shown in [9]. For poloidal flow, there is another complication in addition to the non-constant pressure and poloidal current on each magnetic flux surface. This is because poloidal direction is non-uniform while toroidal direction is uniform for axisymmetric toroidal equilibrium. Since the partial differential equation for the equilibrium with flow has hyperbolic regions and singularity due to the interaction between the poloidal flow and the MHD waves [8], the equilibrium property is complicated [2, 10, 11]. There are several studies of numerical analysis of equilibrium with flow for elliptic regions [12, 13, 14, 15].

In order to describe such equilibrium with strong poloidal flow perturbatively, a set of reduced MHD equilibrium equations for high beta tokamaks with toroidal and poloidal flow comparable to the poloidal sound velocity was derived with asymptotic expansions with respect to the inverse aspect ratio to higher orders [16]. In the reduced MHD, the poloidal and toroidal flows are set to be the same order and compressibility is small. By these orderings, the fast magnetosonic wave is excluded while the slow magnetosonic wave characterized by the poloidal sound velocity is retained. The derivation of equlibrium equations was extended to the two-fluid MHD with finite Larmor radius effects [19, 17, 18]. An analytic solution for the reduced MHD equilibrium was found [20, 21]. The first order solution is identical to that of the static equilibria of [5]. The second order quantities show that the magnetic structure is modified and the pressure isosurfaces depart from the magnetic flux surfaces due to the poloidal flow. They also indicate transition between sub- and super-sonic poloidal flows. While this transition had been analytically studied for low-beta plasmas [2, 10, 11] where magnetic

flux surfaces are approximated to be circular, the analytic solution of [20] indicates non-circular magnetic flux surfaces due to high-beta. This solution was extended to include pressure anisotropy associated with parallel heat flux [22].

The analytic equilibria with flow can be applied to the stability analysis and nonlinear simulations based on the reduced MHD model. They also can be used for benchmark with numerical code to calculate more complicated equilibrium. The analytic studies on equilibrium flow have been still performed by other groups recently [23, 24]. It is noted that, since the flow in [23] is incompressible and the poloidal flow in [24] is slower than the poloidal sound velocity, their solutions do not include the transition between sub- and super-sonic poloidal flows.

Stability of equilibrium with flow is also complicated even in simple equilibrium configurations [2, 25] because of non-Hermitian properties of linear perturbations [26]. However, it is expected that the modifications of the magnetic flux structures and pressure for the transition between sub- and super-sonic poloidal flows affect the stability. To extend the stability theory for more general equilibrium, flux coordinates for high beta toroidal equilibrium with toroidal and poloidal flow will be required since magnetic flux surfaces are non-circular. The corresponding reduced MHD equations for the stability analysis is derived by extending those of [27] for high-beta tokamaks with finite aspect ratio to include density inhomogenity as preliminarily shown in [28].

In this study, we present magnetic flux coordinates for high-beta tokamaks in the presence of toroidal and poloidal flows comparable to the poloidal sound velocity, constructed from the analytic solution for the reduced set of MHD equilibrium equations [20, 21]. We find the flux coordinates from the relation between geometrical and magnetic flux coordinates by extending the flux coordinates for the static equilibria [4]. The solution for the flux coordinates is obtained by solving numerically the high order polynomial equations. By using the flux coordinates, the poloidal distributions of quantities such as the pressure and the terms of the force balance equations on magnetic flux surfaces can be described. The flux coordinates can also be used to calculate the flux average of the pressure. We also obtain the flux coordinates analytically by expanding the relations between geometrical and magnetic flux coordinates with respect to the inverse aspect ratio.

The paper is organized as follows. In section 2, we introduce reduced MHD equations for high beta tokamak equilibrium with flow comparable to the poloidal sound velocity and their analytic solution. In section 3, we obtain flux coordinates from the analytic solution. In section 4, we present poloidal profiles of pressure on magnetic flux surfaces and their dependences on the poloidal Mach number are compared with the poloidal profiles of the terms in the radial force balance. In section 5, we present flux average of pressure, and its dependence on the poloidal Mach number is also discussed. In section 6, an analytic expression for flux coordinates is derived approximately. A summary is given in section 7.

## 2. Analytic high-beta tokamak equilibria with flow

In this section, we briefly introduce the reduced MHD equations for equilibrium with flow in [16] and an analytic solution of the equations in [20, 21]. The equations for ideal MHD equilibria are

$$\nabla \cdot (n\mathbf{v}) = 0, \tag{2}$$

$$m_i n\mathbf{v} \cdot \nabla \mathbf{v} = \mathbf{j} \times \mathbf{B} - \nabla p, \tag{3}$$

$$\mathbf{E} + \mathbf{v} \times \mathbf{B} = 0, \tag{4}$$

$$\nabla \times \mathbf{E} = 0, \tag{5}$$

$$\mu_0 \mathbf{j} = \nabla \times \mathbf{B}, \tag{6}$$

$$\nabla \cdot \mathbf{B} = 0, \tag{7}$$

$$\mathbf{v} \cdot \nabla p + \gamma p \nabla \cdot \mathbf{v} = 0, \tag{8}$$

where $m_i$ is the ion mass, $n$ is the density, $\mathbf{v}$ is the ion flow velocity, $\mathbf{E}$ and $\mathbf{B}$ are the electric and magnetic fields, $\mathbf{j}$ is the current density, $p$ is the pressure, and $\gamma = 5/3$. Here we consider the corresponding toroidal axisymmetric equilibria, where, in cylindrical coordinates $(R, \varphi, Z)$, the magnetic field $\mathbf{B}$ and the current density $\mathbf{j}$ can be written as

$$\mathbf{B} = \nabla\psi(R, Z) \times \nabla\varphi + I(R, Z)\nabla\varphi, \tag{9}$$

$$\mu_0 \mathbf{j} = \nabla I \times \nabla\varphi - \Delta^* \psi \nabla\varphi, \tag{10}$$

where $\psi$ is the poloidal magnetic flux and $\Delta^* \equiv R^2 \nabla \cdot [R^{-2}\nabla]$.

A standard derivation of the generalized GS equation [8, 31] is obtained with the stream function $\Psi$ and the electrostatic potential $\Phi$ defined as

$$n\mathbf{v} = \nabla\Psi(R, Z) \times \nabla\varphi + nRv_\varphi(R, Z)\nabla\varphi, \tag{11}$$

$$\mathbf{E} = -\nabla\Phi. \tag{12}$$

It is shown that

$$\Psi = \Psi(\psi), \tag{13}$$

$$\Phi = \Phi(\psi), \tag{14}$$

$$v_\varphi = \frac{I}{nR}\Psi'(\psi) + R\Phi'(\psi), \tag{15}$$

$$pn^{-\gamma} = S(\psi). \tag{16}$$

However, we follow the procedure of reduced MHD [27] to include low compressibility to obtain the asymptotic expansions of the GS equation as follows. Although the equivalent expansion from the generalized GS equation is not straightforward, the relationship between them will be discussed later in this section.

Equations (2) - (8) are reduced with asymptotic expansions with respect to the inverse aspect ratio $\varepsilon \equiv a/R_0 \ll 1$ where $a$ and $R_0$ are the characteristic scale length of the minor and major radii of a torus, respectively. The following high-beta tokamak orderings for compressible reduced MHD are applied,

$$B_p \sim \varepsilon B_0, \quad p \sim \varepsilon \left(B_0^2/\mu_0\right), \quad |\nabla| \sim 1/a. \tag{17}$$

The energy of flows in the order of the poloidal sound speed $v \sim C_{sp} \equiv (B_p/B_0)(\gamma p/nm_i)^{1/2}$ is the third order of the magnetic energy,

$$m_i n v^2 \sim \varepsilon^2 p \sim \varepsilon^3 \left(B_0^2/\mu_0\right). \tag{18}$$

The toroidal and poloidal flows $v_\varphi$ and $v_p$, respectively, are the same order,

$$v_\varphi \sim v_p \sim C_{sp}. \tag{19}$$

The compressibility is assumed to be weak: $\nabla \cdot \mathbf{v} \sim \varepsilon v/a$. Thus, the flow velocity $\mathbf{v}$ can be written as

$$\mathbf{v} \equiv (1 + x/R_0)\, \nabla U \times (\mathbf{B}/B) + v_\parallel (\mathbf{B}/B). \tag{20}$$

It is shown in Appendix of [27] that (20) obtains correct compressibility up to the order required. The function $U$ is expanded as

$$U(R,Z) = U_1(R,Z) + U_2(R,Z) + \ldots,$$

where $U_2 \sim \varepsilon U_1$, while we need only the leading order quantity of the parallel flow velocity $v_\parallel$. The other variables are also expanded in orders of $\varepsilon$ as

$$\begin{aligned}
\psi(R,Z) &= \psi_1(R,Z) + \psi_2(R,Z) + \psi_3(R,Z) + \ldots, \\
I(R,Z) &= B_0 R_0 + I_1(R,Z) + I_2(R,Z) + I_3(R,Z) + \ldots, \\
p(R,Z) &= p_1(R,Z) + p_2(R,Z) + p_3(R,Z) + \ldots, \\
n(R,Z) &= n_0(R,Z) + n_1(R,Z) + \ldots,
\end{aligned}$$

where $\psi_i \sim \varepsilon^i a R_0 B_0$, $p_i \sim \varepsilon^i B_0^2/\mu_0$ $(i = 1, 2 \ldots)$, and $B_0$ and $R_0$ are constant. Substituting these expansions into equations (2) - (8) and applying the above orderings, the reduced equilibrium equations are obtained order by order in the $(R, Z)$ coordinates. When the equations (2) - (8) are expanded in powers of $\varepsilon$, the coefficient of each power in the equation is separately equal to zero [29]. Although there may be many ways in asymptotic expansions, as mentioned in [29], we take the expansions that the GS equation for $\psi_1$ coincides with that of [5, 6]. The leading order of the momentum balance equation (3) is

$$\nabla \left[ p_1(R,Z) + \frac{B_0}{\mu_0 R_0} I_1(R,Z) \right] = 0 \tag{21}$$

which is the order of $\varepsilon \left(B_0^2/\mu_0\right)/a$ and yields

$$p_1(R,Z) + \frac{B_0}{\mu_0 R_0} I_1(R,Z) = const. \tag{22}$$

It is shown that the following quantities are the functions of $\psi_1$, $p_1(\psi_1)$, $I_1(\psi_1)$, $n_0(\psi_1)$ and $U_1(\psi_1)$, from the relation, for example,

$$(\nabla\psi_1 \times \nabla\varphi) \cdot \nabla p_1(R, Z) = 0. \tag{23}$$

The GS equations for the first order and the second order magnetic flux $\psi_1$ and $\psi_2$, respectively, are given by the projection of the momentum balance equation (3) in the direction of $\nabla\psi = \nabla\psi_1 + \nabla\psi_2 + \ldots$ as

$$\left(\frac{\partial^2}{\partial R^2} + \frac{\partial^2}{\partial Z^2}\right)\psi_1 = -\mu_0 R_0^2 \left(\frac{2x}{R_0}p_1' + g_*'\right) - \left(\frac{I_1^2}{2}\right)', \tag{24}$$

$$\begin{aligned}
&\left(\frac{\partial^2}{\partial R^2} + \frac{\partial^2}{\partial Z^2}\right)\psi_2 + \left[\mu_0 R_0^2 \left(\frac{2x}{R_0}p_1'' + g_*''\right) + \left(\frac{I_1^2}{2}\right)''\right]\psi_2 - \frac{1}{R}\frac{\partial\psi_1}{\partial R} \\
&= M_{Ap}^2 \left(\frac{\partial^2}{\partial R^2} + \frac{\partial^2}{\partial Z^2}\right)\psi_1 + \frac{|\nabla\psi_1|^2}{2}\left(M_{Ap}^2\right)' - \mu_0 R_0^2 \left[\left(\frac{x}{R_0}\right)^2 p_1' + E_*'\right] \\
&\quad + \mu_0 R_0^2 \left[\frac{2x}{R_0}\left(\frac{M_{Ap}^2 p_{2*} - \beta_1 p_{3*}}{\beta_1 - M_{Ap}^2}\right)' - \left(\frac{x}{R_0}\right)^2 \left(\frac{2M_{Ap}^2 \gamma p_1}{\beta_1 - M_{Ap}^2}\right)'\right],
\end{aligned} \tag{25}$$

where $x = R - R_0 \sim a$,

$$\frac{1}{R}\frac{\partial\psi_1}{\partial R} \sim \frac{\psi}{aR_0} \sim \varepsilon\left(\frac{\partial^2}{\partial R^2} + \frac{\partial^2}{\partial Z^2}\right)\psi_1, \tag{26}$$

$$M_{Ap}(\psi_1) \equiv \left[\mu_0 m_i n_0(\psi_1)\right]^{1/2} R_0 U_1'(\psi_1) \tag{27}$$

is the leading order of the poloidal Alfvén Mach number, the ratio between the poloidal flow velocity and the poloidal Alfvén velocity, $\beta_1(\psi_1) \equiv \gamma p_1/(B_0^2/\mu_0)$, and the prime denotes the derivative with respect to $\psi_1$. The other free functions of $\psi_1$ that are $g_*$, $E_*$, $p_{2*}$, and $p_{3*}$, are introduced by eliminating $p_2$, $I_2$, $p_3$ and $I_3$ with the following equations for asymptotic variables

$$p_2 - p_1'\psi_2 + \gamma p_1 \left(\frac{v_\parallel}{B_0 R_0 U_1'} + \frac{2x}{R_0}\right) \equiv p_{2*}(\psi_1), \tag{28}$$

$$B_0 R_0 m_i n_0 U_1' v_\parallel + p_2 - p_1'\psi_2 \equiv p_{3*}(\psi_1), \tag{29}$$

$$p_2 + \frac{B_0}{\mu_0 R_0} I_2 \equiv g_*(\psi_1), \tag{30}$$

$$\begin{aligned}
&p_3 + \frac{B_0 I_3}{\mu_0 R_0} + \frac{I_1}{\mu_0 R_0^2}(I_2 - I_1'\psi_2) + \frac{M_{Ap}^2 |\nabla\psi_1|^2}{2\mu_0 R_0^2} + \left(\frac{x}{R_0}\right)^2 \frac{2M_{Ap}^2 \gamma p_1}{\beta_1 - M_{Ap}^2} - g_*'\psi_2 \\
&\equiv E_*(\psi_1).
\end{aligned} \tag{31}$$

It is noted that the first two terms of LHS of (28) appear from the asymptotic expansion of the convective derivative term of the pressure equation (8),

$$(\nabla U_1 \times \nabla\varphi) \cdot \nabla p_2(R, Z) + (\nabla U_2 \times \nabla\varphi) \cdot \nabla p_1(\psi_1), \tag{32}$$

and the expansion of the toroidal projection of (4),

$$(\nabla\psi_1 \times \nabla\varphi) \cdot \nabla U_2 (R, Z) + (\nabla\psi_2 \times \nabla\varphi) \cdot \nabla U_1(\psi_1) = 0. \tag{33}$$

The first order GS equation (24) coincides with that for static equilibria [5, 6] for the present order of flow while the second order equation (25) includes the effect of flow, which reduces to that of static equiribria [30] in the absence of flow. There is another assumption for the asymptotic expansions that $\left|\beta_1 - M_{Ap}^2\right| \sim \beta_1$.

Other asymptotic variables are obtained from the solution of $\psi_1$ and $\psi_2$ as follows. The second order pressure $p_2$ is obtained as

$$p_2 = p_1'\psi_2 + \frac{(2x/R_0)M_{Ap}^2\gamma p_1}{\beta_1 - M_{Ap}^2} - \frac{M_{Ap}^2 p_{2*} - \beta_1 p_{3*}}{\beta_1 - M_{Ap}^2}. \tag{34}$$

$I_2$ is obtained from (22), (30) and (34) as

$$I_2 = I_1'\psi_2 + \frac{\mu_0 R_0}{B_0}\left[g_* - \frac{(2x/R_0)M_{Ap}^2\gamma p_1}{\beta_1 - M_{Ap}^2} + \frac{M_{Ap}^2 p_{2*} - \beta_1 p_{3*}}{\beta_1 - M_{Ap}^2}\right]. \tag{35}$$

The terms with $(2x/R_0)$ in (34) and (35) show that $p$ and $I$ become non-constant on each magnetic flux surface due to poloidal flow. The parallel flow is obtained as

$$v_\parallel = -\frac{(2x/R_0)\gamma p_1 - (p_{2*} - p_{3*})}{(\beta_1 - M_{Ap}^2)(B_0^2/\mu_0)} M_{Ap} v_A, \tag{36}$$

where $v_A \equiv B_0/\sqrt{\mu_0 n_0 m_i}$. Equation (36) shows that the parallel flow is associated with the poloidal flow. This comes from the ordering of reduced MHD that the toroidal and poloidal flows are comparable and the compressibility is small. The effect of the parallel flow $v_\parallel$ contributes to the second order GS equation (25) implicitly by the coupling with the second order pressure $p_2$ as in (28) and (29). In the leading order, relations between $\Psi$, $\Phi$, and $U$ are

$$\Phi_1'(\psi_1) = -B_0 U_1', \tag{37}$$

$$\Psi_1'(\psi_1) = n_0 R_0 U_1', \tag{38}$$

which cancels the lowest order of the toroidal velocity $v_\varphi$ in (15), which is the order of the sound velocity, as

$$v_{\varphi 0} = \frac{B_0}{n_0}\Psi_1' + R_0\Phi_1' = 0. \tag{39}$$

The leading order of the toroidal velocity is, thus, $v_{\varphi 1} = v_\parallel$. Since two free functions $\Psi$ and $\Phi$ in the standard derivation of the generalized GS equation is degenerated into $U$ as in (37) and (38), the free function for the parallel or toroidal flow independent of the poloidal flow does not exist. Thus, this equilibrium model is mainly for studying the effect of the poloidal flow though the parallel flow also exists. It is noted that if one assumes $p_{2*} \propto M_{Ap}^{-1}$, toroidal flows independent of the poloidal flow can be produced, but such flows contribute to neither the magnetic structure nor non-constant part of

the pressure on magnetic flux surfaces of interest in this study. The second order of $U$ is obtained from (33) as

$$U_2 = U_1'\psi_2 + U_{2*}\left(\psi_1\right), \tag{40}$$

where $U_{2*}$ is a free function of $\psi_1$. The derivation of the reduced equilibrium equations by using $\Psi$ and $\Phi$, including the effects of two-fluid, ion finite Larmor radius and pressure anisotropy, is shown in [19]. The first order density $n_1$ is obtained from the expansion of (2) with (20) as

$$n_1 - n_0'\psi_2 + \frac{n_0 v_\parallel}{B_0 R_0 U_1'} + \frac{2x}{R_0} n_0 \equiv n_{1*}\left(\psi_1\right). \tag{41}$$

Substituting (36) into (41), we obtain

$$n_1 = n_0'\psi_2 + n_{1*}\left(\psi_1\right) + \frac{(2x/R_0)M_{Ap}^2}{\beta_1 - M_{Ap}^2} n_0 - \frac{p_{2*} - p_{3*}}{(\beta_1 - M_{Ap}^2)(B_0^2/\mu_0)} n_0, \tag{42}$$

where $n_{1*}$ is a free function of $\psi_1$. The leading order of the entropy $S$ in (16) is given by $S_1\left(\psi_1\right) = p_1 n_0^{-\gamma}$. The derivation of the GS equations shown here can be applied for the two-fluid MHD with finite Larmor radius effects [17, 18, 19] where the full GS equations have not derived yet since the equations are complicated.

An analytic solution for the set of (24) and (25) can be found for linear profiles of the following free functions [20],

$$p_1 = \varepsilon \left(B_0^2/\mu_0\right) p_{1c}\left(\psi_1/\psi_c\right), \tag{43}$$

$$g_* + \frac{I_1^2}{2\mu_0 R_0^2} = \varepsilon^2 \left(B_0^2/\mu_0\right) g_c \left(\frac{\psi_1}{\psi_c}\right), \tag{44}$$

$$M_{Ap}^2 = \varepsilon M_{Apc}^2\left(\psi_1/\psi_c\right), \tag{45}$$

where $p_{1c}$, $g_c$, and $M_{Apc}^2$ are constant values of the order of unity and $\psi_c$ is a normalization constant of $\psi_1$. Here, we consider a simple case where $p_{2*} = p_{3*} = E_* = 0$. The fixed boundary conditions for $\psi_1$ and $\psi_2$ are given by assuming circular cross section as

$$\psi_1(R_0 + a\cos\theta, a\sin\theta) = 0, \tag{46}$$

$$\psi_2(R_0 + a\cos\theta, a\sin\theta) = 0, \tag{47}$$

where $-\pi \le \theta \le \pi$. We then apply the following normalization

$$\left(R - R_0\right)/a \equiv \overline{x}, \qquad Z/a \equiv \overline{z}, \tag{48}$$

$$a/R_0 \equiv \varepsilon, \tag{49}$$

$$\psi_1/\psi_c \equiv \overline{\psi}_1\left(\overline{x}, \overline{z}\right), \tag{50}$$

$$\psi_2/\psi_c \equiv \varepsilon\overline{\psi}_2\left(\overline{x}, \overline{z}\right), \tag{51}$$

and

$$\psi_c/B_0 R_0 a \equiv \varepsilon \bar{B}_p. \tag{52}$$

In the following, we omit the overbars. Equations (24) and (25) are rewritten as

$$\left(\frac{\partial^2}{\partial x^2}+\frac{\partial^2}{\partial z^2}\right)\psi_1 = -\frac{2xp_{1c}}{B_p^2}-\frac{g_c}{B_p^2}, \tag{53}$$

$$\begin{aligned}&\left(\frac{\partial^2}{\partial x^2}+\frac{\partial^2}{\partial z^2}\right)\psi_2-\frac{\partial\psi_1}{\partial x}\\ &= M_{Apc}^2\psi_1\left(\frac{\partial^2}{\partial x^2}+\frac{\partial^2}{\partial z^2}\right)\psi_1+\frac{|\nabla\psi_1|^2}{2}M_{Apc}^2\\ &\quad-\frac{x^2p_{1c}}{B_p^2}\left(1+\frac{2\gamma M_{Apc}^2}{\gamma p_{1c}-M_{Apc}^2}\right).\end{aligned} \tag{54}$$

The analytic solution of

$$\psi(x,z)\simeq\psi_1(x,z)+\varepsilon\psi_2(x,z) \tag{55}$$

is written in the coordinates $(x,z)$ as

$$\psi_1(x,z)=\frac{g_c}{4B_p^2}\frac{1-3{\Delta^2}_{s1}+2\Delta_{s1}x}{1-3{\Delta^2}_{s1}}\left(1-x^2-z^2\right), \tag{56}$$

$$\begin{aligned}\psi_2(x,z)=&-\frac{g_c}{16B_p^2}\frac{1-x^2-z^2}{1-3{\Delta^2}_{s1}}\left\{-2\Delta_{s1}\left[x^2+z^2+\frac{\gamma M_{Apc}^2}{\gamma p_{1c}-M_{Apc}^2}(1+x^2+z^2)\right]\right.\\ &+\frac{M_{Apc}^2}{8}\frac{g_c}{B_p^2}\left(1-3{\Delta^2}_{s1}\right)\left\{3\left(x^2+z^2\right)-5\right.\\ &\left.\left.+\frac{1}{9}\left(\frac{2\Delta_{s1}}{1-3{\Delta^2}_{s1}}\right)^2\left[13\left(x^2+z^2\right)^2-14\left(x^2+z^2\right)-5\right]\right\}\right.\\ &+x\left\{-1+3{\Delta^2}_{s1}+\frac{M_{Apc}^2}{2}\frac{g_c}{B_p^2}\Delta_{s1}\left[3\left(x^2+z^2\right)-4\right]\right\}\\ &+2\Delta_{s1}\left(x^2-z^2\right)\left\{-1-\frac{4}{3}\frac{\gamma M_{Apc}^2}{\gamma p_{1c}-M_{Apc}^2}\right.\\ &\left.\left.+\frac{M_{Apc}^2}{24}\frac{g_c}{B_p^2}\frac{\Delta_{s1}}{1-3{\Delta^2}_{s1}}\left[9\left(x^2+z^2\right)-11\right]\right\}\right\},\end{aligned} \tag{57}$$

where $\Delta_{s1}$ is the shift of the magnetic axis of $\psi_1$ from the geometric axis,

$$\left.\frac{\partial\psi_1}{\partial x}\right|_{(x,z)=(\Delta_{s1},0)}=0, \tag{58}$$

$$\Delta_{s1}=\frac{-1+\sqrt{1+3(p_{1c}/g_c)^2}}{3(p_{1c}/g_c)}. \tag{59}$$

The solution for $\psi_1$, (56), coincides with that for static equilibria [5, 6], and the solution for $\psi_2$, (57), reduces to that of static equiribria [30] in the absence of flow. The pressure normalized with $\varepsilon B_0^2/\mu_0$ is obtained from $\psi_1$ and $\psi_2$ as

$$p=p_{1c}\left(\psi_1+\varepsilon\psi_2+\varepsilon\frac{2\gamma M_{Apc}^2}{\gamma p_{1c}-M_{Apc}^2}\psi_1 x\right). \tag{60}$$

The third term in the parentheses of the RHS of (60) is non-constant on each flux surface $\psi \simeq \psi_1 + \varepsilon\psi_2 = const.$ in the presence of the poloidal flow. The quantity $M_{Apc}^2/\gamma p_{1c}$ reads as the square of the poloidal Mach number, the ratio between the poloidal flow velocity, and the poloidal sound velocity. We define the poloidal flow with $M_{Apc}^2/\gamma p_{1c} < 1$ as sub-sonic and $M_{Apc}^2/\gamma p_{1c} > 1$ as super-sonic. The poloidal sound velocity is the characteristic velocity of the slow magnetosonic wave. This order of poloidal flow had been analytically studied for low-beta plasmas [2, 10, 11] to model transport barriers or pedestals associated with transonic poloidal flows. The analytic solutions (56) and (57) show that the magnetic flux surfaces are non-circular even when the poloidal cross-section of plasma region is circular. This is the key feature of high-beta equilibrium and the reason why magnetic flux coordinates suitable to stability analysis are investigated in this paper. Since the flow in [23] is incompressible and the poloidal flow in [24] is the order of $\sqrt{\varepsilon}$ slower than the poloidal sound velocity, their analytic solutions do not include the interaction between poloidal flow and the slow magnetosonic wave. In the analytic solution shown here describes the behavior of poloidal flow comparable to poloidal sound velocity in high-beta equilibrium that cannot be described by other models, though the toroidal flow is not independently defined.

In the next section, we show the flux coordinates obtained from the solutions (56) and (57) for sub- and super-sonic poloidal flows. In the following sections, we choose the parameters $p_{1c} = 3.2$, $g_c = 4.0$, $\varepsilon = 0.1$, and $B_p = 1.0$ as in [20]. It is shown in [22] that the analytic solution shown here is extended to include pressure anisotropy associated with parallel heat flux for nearly collisionless tokamaks. This includes isothermal electron pressure in a limit. The isothermal pressure only changes the poloidal sound velocity quantitatively from $(B_p/B_0)(\gamma p/nm_i)^{1/2}$ to $(B_p/B_0)[(\gamma p_i + p_e)/nm_i]^{1/2}$ in the case of adiabatic ion pressure and isothermal electron pressure. In the present study, we consider adiabatic pressure to obtain the standard formulation. Extension of the magnetic flux coordinates derived in the present paper to non-adiabatic pressure in [22] is straightforward but requires more lengthy formulation.

## 3. Flux coordinates

The flux coordinates obtained in [4] in the case of circular poloidal cross section at the boundary are reproduced from the first order magnetic flux $\psi_1$ in (56). The flux coordinates $(\xi,\Theta)$ are related to $(x, z)$ as

$$\left(1 - \xi^2 \cos^2\Theta\right) \psi_{11}\left(\Delta_{s1}\right) = \psi_{11}\left(x\right), \tag{61}$$

$$\left(-\xi^2 \sin^2\Theta\right) \psi_{11}\left(\Delta_{s1}\right) = \psi_{12}\left(x, z\right), \tag{62}$$

where $\psi_1$ has been split as

$$\psi_1\left(x, z\right) = \psi_{11}\left(x\right) + \psi_{12}\left(x, z\right), \tag{63}$$

$$\psi_{11}\left(x\right) = \frac{g_c}{4B_p^2} \frac{1 - 3{\Delta^2}_{s1} + 2\Delta_{s1} x}{1 - 3{\Delta^2}_{s1}} \left(1 - x^2\right), \tag{64}$$

and

$$\psi_{12}(x,z) = -\frac{g_c}{4B_p^2}\frac{1-3{\Delta^2}_{s1}+2\Delta_{s1}x}{1-3\Delta_{s1}^2}z^2. \tag{65}$$

Equation (61) is a cubic equation for $x\,(\xi,\Theta)$ and (62) is a quadratic equation for $z\,(\xi,\Theta)$ which are analytically solved as

$$\begin{aligned} x = x_1 \equiv \Delta_{s1} + & \frac{1+3\Delta_{s1}^2}{6\Delta_{s1}}\{-1 \\ & +2\cos\left\{\frac{2}{3}\arccos\left[\frac{3\sqrt{3}\Delta_{s1}\left(1-\Delta_{s1}^2\right)}{\left(1+3\Delta_{s1}^2\right)^{3/2}}\xi\cos\Theta\right]\right\}\Bigg\}, \end{aligned} \tag{66}$$

$$z = z_1 \equiv \frac{1-\Delta_{s1}^2}{\sqrt{1-3\Delta_{s1}^2+2\Delta_{s1}x_1}}\xi\sin\Theta. \tag{67}$$

The flux coordinates $(\xi,\Theta)$ constitute a non-orthogonal coordinate system in the poloidal cross section. The $\xi$ coordinate represents flux surfaces and ranges from $\xi = 0$ at the magnetic axis $\Delta_{s1}$ of $\psi_1$ to $\xi = 1$ at the boundary. The $\Theta$ coordinate represents the poloidal angle where $\Theta = 0$ for outer midplane, $\Theta = \pm\pi$ for inner midplane, and $-\pi < \Theta < 0$ for lower half and $0 < \Theta < \pi$ for upper half. This coordinate system is different from the straight field line and the constant arc length coordinate systems which are obtained numerically [4, 32].

To extend the above coordinates to the magnetic flux including the second order, $\psi \simeq \psi_1 + \varepsilon\psi_2$, in the presence of flow, we add the contribution of $\psi_2$ into (61) and (62) by splitting $\psi_2$ in the similar manner as $\psi_1$ such as

$$\psi_2(x,z) = \psi_{21}(x) + \psi_{22}(x,z) \tag{68}$$

$$\begin{aligned} \psi_{21}(x) = & -\frac{g_c}{16B_p^2}\frac{1-x^2}{1-3{\Delta^2}_{s1}}\left\{-x\left(4\Delta_{s1}x+1-3{\Delta^2}_{s1}\right)\right. \\ & -\frac{2\Delta_{s1}}{3}\frac{\gamma M_{Apc}^2}{\gamma p_{1c}-M_{Apc}^2}\left(3+7x^2\right) \\ & +\frac{M_{Apc}^2}{2}\frac{g_c}{B_p^2}\left[\frac{1}{4}\left(1-3{\Delta^2}_{s1}\right)\left(3x^2-5\right)+\Delta_{s1}(3x^2-4)x\right. \\ & \left.\left.+\frac{1}{18}\frac{{\Delta^2}_{s1}}{1-3{\Delta^2}_{s1}}(53x^4-61x^2-10)\right]\right\} \end{aligned} \tag{69}$$

$$\begin{aligned} \psi_{22}(x,z) = & -\frac{g_c}{16B_p^2}\frac{z^2}{1-3\Delta_{s1}^2}\left\{\left(1-x^2\right)\right. \\ & \times\left\{-2\Delta_{s1}\left(1+\frac{\gamma M_{Apc}^2}{\gamma p_{1c}-M_{Apc}^2}\right)\right. \\ & +\frac{M_{Apc}^2}{8}\frac{g_c}{B_p^2}\left(1-3{\Delta^2}_{s1}\right) \\ & \left.\left.\times\left[3+\frac{1}{9}\left(\frac{2\Delta_{s1}}{1-3{\Delta^2}_{s1}}\right)^2\left(26x^2+13z^2-14\right)\right]\right. \end{aligned}$$

$$
\begin{aligned}
&+\frac{3M_{Apc}^2}{4}\frac{g_c}{B_p^2}\Delta_{s1}x\left(2+\frac{\Delta_{s1}}{1-3{\Delta^2}_{s1}}x\right)\Bigg\}\\
&-2\Delta_{s1}\left(1-z^2\right)\Bigg\{-1-\frac{4}{3}\frac{\gamma M_{Apc}^2}{\gamma p_{1c}-M_{Apc}^2}\\
&+\frac{M_{Apc}^2}{24}\frac{\Delta_{s1}}{1-3\Delta_{s1}^2}\frac{g_c}{B_p^2}\left[9\left(x^2+z^2\right)-11\right]\Bigg\}\\
&+2\Delta_{s1}\left[x^2+z^2+\frac{\gamma M_{Apc}^2}{\gamma p_{1c}-M_{Apc}^2}\left(1+x^2+z^2\right)\right]\\
&-\frac{M_{Apc}^2}{8}\frac{g_c}{B_p^2}\left(1-3\Delta_{s1}^2\right)\Big\{3\left(x^2+z^2\right)-5\\
&+\frac{1}{9}\left(\frac{2\Delta_{s1}}{1-3\Delta_{s1}^2}\right)^2\left[13\left(x^2+z^2\right)^2-14\left(x^2+z^2\right)-5\right]\Bigg\}\\
&-x\left\{-1+3\Delta_{s1}^2+\frac{M_{Apc}^2}{2}\frac{g_c}{B_p^2}\Delta_{s1}\left[3\left(x^2+z^2\right)-4\right]\right\}\Bigg\}. \qquad (70)
\end{aligned}
$$

We, then, obtain

$$\left(1-\xi^2\cos^2\Theta\right)\left[\psi_{11}\left(\Delta_s\right)+\varepsilon\psi_{21}\left(\Delta_s\right)\right]=\psi_{11}\left(x\right)+\varepsilon\psi_{21}\left(x\right), \qquad (71)$$

$$\left(-\xi^2\sin^2\Theta\right)\left[\psi_{11}\left(\Delta_s\right)+\varepsilon\psi_{21}\left(\Delta_s\right)\right]=\psi_{12}\left(x,z\right)+\varepsilon\psi_{22}\left(x,z\right), \qquad (72)$$

where $\Delta_s$ is the shift of the magnetic axis of $\psi\simeq\psi_1+\varepsilon\psi_2$ from the geometric axis,

$$\left.\frac{d\psi_{11}}{dx}\right|_{x=\Delta_s}+\varepsilon\left.\frac{d\psi_{21}}{dx}\right|_{x=\Delta_s}=0. \qquad (73)$$

We, first, find $\Delta_s$ by solving (73), and solve (71) and (72) with respect to $(x,z)$ for given $(\xi,\Theta)$. Since (71) - (73) are high order polynomial equations, solutions are obtained numerically with the Newton method. Although $\Delta_s$ was also obtained by asymptotic expansions with respect to $\varepsilon$ in [20, 21], it must be calculated from (73) in order to solve (71) and (72) rigorously.

Figure 1 shows the dependence of $\Delta_s$ on the poloidal Mach number. Compared with $\Delta_{s1}$, the shift is enhanced due to the contribution of the second order magnetic flux $\psi_2$ for sub-sonic poloidal flow, including static equilibrium, and increase with the poloidal Mach number. There is a transition across $M_{Apc}^2/\gamma p_{1c}=1$. The vicinity of this point must be excluded since the assumption $\left|\beta_1-M_{Ap}^2\right|\sim\beta_1$ is violated or a separatrix appears in the plasma region [20, 21]. For super sonic flow, $\Delta_s$ is less than $\Delta_{s1}$.

To find the roots of $x$ and $z$ that are originated from those for static equilibrium, (71) and (72) are solved for $[x\left(\xi,\Theta\right),z\left(\xi,\Theta\right)]$, $0\leq\xi\leq1$, and $-\pi\leq\Theta\leq\pi$, by using $(x_1,z_1)$ in (66) and (67) as initial guesses for the Newton method and the restrictions $x^2+z^2\leq1$, $x<\Delta_s$ for $-\pi\leq\Theta<-\pi/2$ and $\pi/2<\Theta\leq\pi$, $x>\Delta_s$ for $-\pi/2<\Theta<\pi/2$, $z<0$ for $-\pi<\Theta<0$, $z>0$ for $0<\Theta<\pi$, $x=\Delta_s$ for $\Theta=\pm\pi/2$, and $z=0$ for $\Theta=0$ and $\pm\pi$. The flux coordinates $(\xi,\Theta)$ obtained from $\psi\simeq\psi_1+\varepsilon\psi_2$ also constitute a non-orthogonal coordinates in the poloidal cross section. The $\xi$ coordinate represents flux

surfaces and ranges from $\xi = 0$ at the magnetic axis $\Delta_s$ to $\xi = 1$ at the boundary. The $\Theta$ coordinate represents the poloidal angle where $\Theta = 0$ for outer midplane, $\Theta = \pm\pi$ for inner midplane, $-\pi < \Theta < 0$ for lower half, and $0 < \Theta < \pi$ for upper half.

Figures 2 - 4 show the flux coordinates $(\xi, \Theta)$ in the poloidal cross section obtained from $\psi \simeq \psi_1 + \varepsilon\psi_2$ by solving (71) and (72) for $M^2_{Apc}/\gamma p_{1c} = 0$ (static equilibrium), 0.5 (sub-sonic poloidal flow) and 2.5 (super-sonic poloidal flow), respectively, compared with those obtained from $\psi_1$, (66) and (67). Flux surfaces for $\xi < 1$ become non-circular because of high-beta. For the static equilibrium $M^2_{Apc}/\gamma p_{1c} = 0$ (figure 2), the contribution of the second order magnetic flux modifies the flux coordinates along with the shift of the magnetic axis from $\Delta_{s1}$ to $\Delta_s$. The flux coordinates in figures 3 and 4 indicate modification due to flow. For sub-sonic poloidal flow $M^2_{Apc}/\gamma p_{1c} = 0.5$ (figure 3), the modification mainly occurs in the inside region of a torus. The $\xi$ coordinate is shifted toward the magnetic axis in the core region $\xi < 0.8$. The $\Theta$ coordinate at $\Theta = \pm 0.9\pi$ is shifted toward the outer midplane $\Theta = \pm\pi$. For super-sonic poloidal flow $M^2_{Apc}/\gamma p_{1c} = 2.5$ (figure 4), the modification occurs in the whole region. The $\xi$ coordinate is shifted toward the magnetic axis for $\xi < 1$. The $\Theta$ coordinate in the upper (lower) half is shifted toward $\Theta = \pi/2$ ($\Theta = -\pi/2$). For applicability to stability analysis, both of the modication of mode structure and the fluxcoordinates due to flow should be considered.

In sections 4 and 5, properties of static equilibrium, equilibria with sub- and super-sonic poloidal flows are compared with each other by using the flux coordinates of figures 2 - 4.

## 4. Poloidal profiles on magnetic surfaces

As an application of flux coordinates, we present poloidal profiles of equilibrium quantities on flux surfaces. Figures 5 - 7 show the pressure profiles, obtained from (60), in the poloidal angle $\Theta$ on each flux surface, $\xi = const.$, for $M^2_{Apc}/\gamma p_{1c} = 0$, 0.5, and 2.5, respectively. For static equilibrium $M^2_{Apc}/\gamma p_{1c} = 0$, the pressure is constant on each flux surface (figure 5). The pressure is peaked at $\Theta = 0$, the outer midplane, for sub-sonic flow $M^2_{Apc}/\gamma p_{1c} = 0.5$ (figure 6) while it is peaked at $\Theta = \pm\pi$, the inner midplane, for super-sonic flow $M^2_{Apc}/\gamma p_{1c} = 2.5$ (figure 7). In both cases, the pressure becomes maximum at $\xi > 0$. This is consistent with the analysis of the shift of the pressure maximum that is outward for sub-sonic flow and inward for super-sonic flow from the magnetic axis [20, 21] and gives more detailed description of pressure profiles of equilibrium with flow.

To study the mechanism of structures of equilibrium pressure, we compare the poloidal profiles of the terms in the radial force balance equations (53) and (54) on flux surfaces. For the present case where $p_{2*} = p_{3*} = E_* = 0$, we examine the dependence of the forces of flow, poloidal magnetic field and pressure on the poloidal Mach number.

The first order force balance equation is obtained from (53) as

$$F_{B1} + F_{p1} = \frac{g_c}{B_p^2}, \tag{74}$$

where the RHS is the sum of the forces of the toroidal magnetic field and second order pressure, kept constant, $g_c/B_p^2 = 4.0$, and the forces of the poloidal magnetic field and pressure are, respectively,

$$F_{B1} = -\left(\frac{\partial^2}{\partial x^2} + \frac{\partial^2}{\partial z^2}\right)\psi_1, \tag{75}$$

$$F_{p1} = -\frac{2xp_{1c}}{B_p^2}. \tag{76}$$

The second order force balance equation is obtained from (54) as

$$F_v + F_{B2} + F_{p2} = 0, \tag{77}$$

where the forces of the inertia of poloidal flow, poloidal magnetic field and pressure are, respectively,

$$F_v = M_{Apc}^2\psi_1\left(\frac{\partial^2}{\partial x^2} + \frac{\partial^2}{\partial z^2}\right)\psi_1 + \frac{|\nabla\psi_1|^2}{2}M_{Apc}^2, \tag{78}$$

$$F_{B2} = -\left(\frac{\partial^2}{\partial x^2} + \frac{\partial^2}{\partial z^2}\right)\psi_2 + \frac{\partial\psi_1}{\partial x}, \tag{79}$$

$$F_{p2} = -\frac{x^2p_{1c}}{B_p^2}\left(1 + \frac{2\gamma M_{Apc}^2}{\gamma p_{1c} - M_{Apc}^2}\right). \tag{80}$$

The RHS of (77) is zero since we have assumed $p_{2*} = p_{3*} = E_* = 0$ in (25) for simplicity. The contribution of the toroidal magnetic field for this order appears in the poloidal force balance (31) and balances with the other terms. The inertial force of flow (78) does not include the contribution of toroidal flow since the toroidal curvature is small. The second term in the parentheses of the pressure force (80) is the contribution of $p_2$. Equations (28) and (29) show that $p_2$ is coupled with poloidal flow, $U_1$, and the toroidal flow, $v_\parallel$, through the convection due to the poloidal flow and compression. Since these equations are projections along $\nabla\psi$ and $\psi$ is spatially decreasing in all directions from the magnetic axis, the positive signs in the LHSs of (74) and (77) mean the forces toward the magnetic axis. We examine the cases for $M_{Apc}^2/\gamma p_{1c} = 0$ (static equilibrium), 0.5 (sub-sonic poloidal flow), and 2.5 (super-sonic poloidal flow).

Figure 8 shows the poloidal profiles of the first order forces in (74) on different magnetic flux surfaces for $M_{Apc}^2/\gamma p_{1c} = 0$. The averages in $\Theta$ show the force balance in the minor radius of the torus while the variations in $\Theta$ with the period $2\pi$ show the force balance in the major radius. It is noted that the poloidal profiles for $M_{Apc}^2/\gamma p_{1c} = 0.5$ and 2.5 are omitted here since (74) does not include the effect of flow and only small quantitative changes in the profiles of the first order forces occur due to changes of magnetic flux $\psi$ when the flow is included. Figure 8 (a) indicates that, at $\xi = 0.1$

near the magnetic axis, the pressure force $F_{p1}$ is outward from the magnetic axis in the minor radius for all $\Theta$ due to the poloidal curvature and the amplitude is maximum in the outer midplane, $\Theta = 0$, and minimum in the inner midplane, $\Theta = \pm\pi$, due to the outward force in the major radius by the toroidal curvature. The direction and the variation of the force of poloidal magnetic field $F_{B1}$ is opposite to $F_{p1}$ to balance. In the outer region from the magnetic axis $\xi = 0.9$ [figure 8 (b)], on the other hand, $F_{p1}$ in the inner midplane $\Theta = \pm\pi$ is inward to the magnetic axis in the minor radius since the pressure force due to the toroidal curvature becomes larger than that due to the poloidal curvature.

Figures 9 - 11 show the poloidal profiles of the second order forces in (77) multiplied by $\varepsilon$, on different magnetic flux surfaces for $M^2_{Apc}/\gamma p_{1c} = 0$, 0.5, and 2.5, respectively. Figure 9 shows the small correction of each force due to the higher order terms for the static equilibrium $M^2_{Apc}/\gamma p_{1c} = 0$. The pressure force $F_{p2}$ is outward from the magnetic axis due to the poloidal curvature with variations due to the toroidal curvature and balances with the force of poloidal magnetic field $F_{B2}$. The variations in the poloidal angle $\Theta$ have the period $2\pi$ at $\xi = 0.1$ while the variations with the period $\pi$ are relevant at $\xi = 0.9$, which come from the $x^2$ dependence of each force. Figures 10 and 11 indicate large contributions of poloidal flow to the second order force balance (77). For the sub-sonic poloidal flow $M^2_{Apc}/\gamma p_{1c}$ =0.5 (figure 10), the force of flow $F_v$ is outward from the magnetic axis to the boundary except for the edge region $\xi = 0.9$. The pressure force $F_{p2}$ is outward from the magnetic axis as in the static case $M^2_{Apc}/\gamma p_{1c} = 0$ (figure 9). In figure 10 (a), $F_v$ in the inner region $\xi = 0.1$ acts as the centrifugal force due to poloidal curvature, and the sum of $F_v$ and $F_{p2}$, outward from the magnetic axis in the minor radius on average, balance with inward $F_{B2}$. Figure 10 (b) shows that $F_v$ in the edge region $\xi = 0.9$ acts as the dynamic pressure force and the sum of $F_v$ and $F_{B2}$, inward to the magnetic axis on average, balance with outward $F_{p2}$. For the super-sonic poloidal flow $M^2_{Apc}/\gamma p_{1c}$ =2.5 (figure 11), $F_v$ is outward from the magnetic axis except for the edge region $\xi = 0.9$, as for sub-sonic flow. However, the direction of $F_{p2}$ becomes opposite to that of the static equilibrium. The force of flow $F_v$ act as centrifugal force due to poloidal curvature and balances with the sum of $F_{B2}$ and $F_{p2}$ in the core region $\xi = 0.1$ [figure 11 (a)], and the sum of $F_v$ acting as the dynamic pressure and $F_{p2}$ balances with $F_{B2}$ in the edge region $\xi = 0.9$ [figure 11 (b)].

There are transitions between sub-sonic and super-sonic poloidal flows both in the toroidal and poloidal curvature effects. Figure 12 compares the poloidal profiles of the second order pressure force $F_{p2}$ at $\xi = 0.1$ for $M^2_{Apc}/\gamma p_{1c} = 0$, 0.5, and 2.5 with each other. The variations in $\Theta$ show that the sub-sonic poloidal flow enhances the outward component in the major radius of the torus in $F_{p2}$ due to the effect of toroidal curvature while the super-sonic poloidal flow changes its direction. This transition of the toroidal curvature effect comes from compressibility of flow [20] and results in the transition of the poloidal profile of the pressure shown in figures 6 and 7 that the pressure is peaked in the outer mid-plane for sub-sonic poloidal flow and peaked in the inner mid-plane for super-sonic poloidal flow. The second order pressure force $F_{p2}$ on average in $\Theta$ show

the transition of the pressure force in the minor radius of the torus due to the poloidal curvature effect. This transition of the effect of poloidal curvature will be discussed in comparison with the flux average of pressure in the next section.

## 5. Flux average of pressure

The flux coordinates can also be used to calculate flux averages. The flux average of the pressure is given by

$$\langle p\rangle(\xi)=\int_{-\pi}^{\pi}p(\xi,\Theta)\,Dd\Theta/\int_{-\pi}^{\pi}Dd\Theta, \tag{81}$$

where

$$D=\frac{\partial x}{\partial\xi}\frac{\partial z}{\partial\Theta}-\frac{\partial x}{\partial\Theta}\frac{\partial z}{\partial\xi}. \tag{82}$$

From (71) and (72),

$$\frac{\partial x}{\partial\xi}=\frac{\psi_{11}(\Delta_s)+\varepsilon\psi_{21}(\Delta_s)}{\psi'_{11}(x)+\varepsilon\psi'_{21}(x)}\left(-2\xi\cos^2\Theta\right), \tag{83}$$

$$\frac{\partial x}{\partial\Theta}=\frac{\psi_{11}(\Delta_s)+\varepsilon\psi_{21}(\Delta_s)}{\psi'_{11}(x)+\varepsilon\psi'_{21}(x)}\left(2\xi^2\cos\Theta\sin\Theta\right), \tag{84}$$

$$\frac{\partial z}{\partial\xi}=-\frac{2\xi\left[\psi_{11}(\Delta_s)+\varepsilon\psi_{21}(\Delta_s)\right]}{\frac{\partial\psi_{12}}{\partial z}+\varepsilon\frac{\partial\psi_{22}}{\partial z}}\left[\sin^2\Theta-\frac{\frac{\partial\psi_{12}}{\partial x}+\varepsilon\frac{\partial\psi_{22}}{\partial x}}{\psi'_{11}(x)+\varepsilon\psi'_{21}(x)}\cos^2\Theta\right], \tag{85}$$

$$\frac{\partial z}{\partial\Theta}=-\frac{2\xi^2\sin\Theta\cos\Theta\left[\psi_{11}(\Delta_s)+\varepsilon\psi_{21}(\Delta_s)\right]}{\frac{\partial\psi_{12}}{\partial z}+\varepsilon\frac{\partial\psi_{22}}{\partial z}}\left[1+\frac{\frac{\partial\psi_{12}}{\partial x}+\varepsilon\frac{\partial\psi_{22}}{\partial x}}{\psi'_{11}(x)+\varepsilon\psi'_{21}(x)}\right]. \tag{86}$$

Substituting (83) - (86) into (82), we obtain

$$D=\frac{4\xi^3\sin\Theta\cos\Theta\left[\psi_{11}(\Delta_s)+\varepsilon\psi_{21}(\Delta_s)\right]^2}{\left[\psi'_{11}(x)+\varepsilon\psi'_{21}(x)\right]\left(\frac{\partial\psi_{12}}{\partial z}+\varepsilon\frac{\partial\psi_{22}}{\partial z}\right)}. \tag{87}$$

The flux average of the pressure, (81), is calculated with numerical integration with respect to $\Theta$ by using the solution of $[x(\xi,\Theta),z(\xi,\Theta)]$ obtained in section 3. We employ the Gaussian quadrature with 1000 intervals as a numerical integration method. Figure 13 compares the radial profiles of the flux surface average of the pressure for $M^2_{Apc}/\gamma p_{1c}=0$, 0.5, and 2.5 with each other. They are normalized with the values of pressure at $\xi=0$. Though the differences are small, the profile of the flux surface average of the pressure is more peaked near the magnetic axis for sub-sonic poloidal flow $M^2_{Apc}/\gamma p_{1c}=0.5$ while it is broader for super-sonic poloidal flow $M^2_{Apc}/\gamma p_{1c}=2.5$, compared with that for the static equilibrium $M^2_{Apc}/\gamma p_{1c}=0$. Comparing the flux average of the pressure (figure 13) with the second-order force balances (figure 12), the pressure is more peaked and the second-order force of pressure is outward in the minor radius for sub-sonic poloidal flow while the pressure is broader and the second-order force of pressure is inward for super-sonic poloidal flow. Thus the flux average of pressure is compressed to concentrate near the magnetic axis due to the poloidal curvature by sub-sonic poloidal flow while it is decompressed by super-sonic poloidal flow.

## 6. Analytic flux coordinates

The flux coordinates can be obtained analytically by expanding the relations between geometrical and magnetic flux coordinates, (71) and (72), with respect to the inverse aspect ratio. We apply asymptotic expansions to the geometric coordinates $[x(\xi,\Theta), z(\xi,\Theta)]$ as

$$x \simeq x_1 + \varepsilon x_2, \tag{88}$$

$$z \simeq z_1 + \varepsilon z_2, \tag{89}$$

and expanding $\Delta_s$ as

$$\Delta_s \simeq \Delta_{s1} + \varepsilon \Delta_{s2}, \tag{90}$$

where $x$, $x_1$, $x_2$, $z$, $z_1$, $z_2$, $\Delta_s$, $\Delta_{s1}$ and $\Delta_{s2}$ are normalized quantities with the minor radius $a$ and, from [20],

$$\Delta_{s2} = -\psi'_{21}(\Delta_{s1}) / \psi''_{11}(\Delta_{s1}). \tag{91}$$

In the leading order, Eqs (71) and (72) are

$$\left(1 - \xi^2 \cos^2\Theta\right) \psi_{11}(\Delta_{s1}) = \psi_{11}(x_1), \tag{92}$$

$$\left(-\xi^2 \sin^2\Theta\right) \psi_{11}(\Delta_{s1}) = \psi_{12}(x_1, z_1), \tag{93}$$

which are the same as (61) and (62) and the solutions of $x_1$ and $z_1$ are (66) and (67), respectively. The first order equations are

$$\left(1 - \xi^2 \cos^2\Theta\right) \psi_{21}(\Delta_{s1}) = \psi'_{11}(x_1)\, x_2 + \psi_{21}(x_1), \tag{94}$$

$$\left(-\xi^2 \sin^2\Theta\right) \psi_{21}(\Delta_{s1}) = \left.\frac{\partial \psi_{12}}{\partial x}\right|_{(x,z)=(x_1,z_1)} x_2 + \psi_{22}(x_1, z_1) \tag{95}$$

$$+ \left.\frac{\partial \psi_{12}}{\partial z}\right|_{(x,z)=(x_1,z_1)} z_2, \tag{96}$$

which yield

$$x_2 = \left[\psi'_{11}(x_1)\right]^{-1} \left[\left(1 - \xi^2 \cos^2\Theta\right) \psi_{21}(\Delta_{s1}) - \psi_{21}(x_1)\right], \tag{97}$$

$$z_2 = \left( \left.\frac{\partial \psi_{12}}{\partial z}\right|_{(x,z)=(x_1,z_1)} \right)^{-1} \times \left[ \left(-\xi^2 \sin^2\Theta\right) \psi_{21}(\Delta_{s1}) - \left.\frac{\partial \psi_{12}}{\partial x}\right|_{(x,z)=(x_1,z_1)} x_2 - \psi_{22}(x_1, z_1) \right]. \tag{98}$$

It is noted that zeros at $x_1 = \Delta_{s1}$ and $z_1 = 0$ in the denominators of (97) and (98), respectively, are eliminated by their numerators to obtain $x_2 = \Delta_{s2}$ and $z_2 = 0$.

Figures 14 - 16 show the flux coordinate systems constructed from analytic representation of (88) and (89) with (66), (67), (97), and (98), compared with numerical solutions for $M^2_{Apc}/\gamma p_{1c} = 0$, 0.5, and 2.5, respectively. The analytic flux coordinates

well agree with the numerical solution for $M_{Apc}^2/\gamma p_{1c} = 0$ and 0.5 (figures 14 and 15). For $M_{Apc}^2/\gamma p_{1c} = 2.5$ (figure 16), the modification of the magnetic flux coordinates qualitatively agree with the numerical solution mentioned in section 3 although $M_{Apc}^2$ becomes large compared to the ordering $M_{Apc}^2 \sim 1$ for $p_{1c} = 3.2$ in the present case, which is not essential for the transition between sub- and super-sonic poloidal flows.

## 7. Summary

We have obtained magnetic flux coordinates from the analytic solution for the reduced MHD equilibrium equations in the presence of flow comparable to the poloidal sound velocity for high-beta tokamaks. The flux coordinates represent non-circular magnetic flux surfaces and indicate modification due to flow. We have shown the poloidal distributions of the pressure on each magnetic flux surface by using magnetic flux coordinates. We have shown from the profiles of the terms in the radial force balance equations that there are transitions between sub- and super-sonic poloidal flows both in the toroidal and poloidal curvature effects on the radial force balance. We have also obtained the flux average of the pressure with the magnetic flux coordinates. Though the differences are small, the profile of the flux surface average of the pressure is more peaked near the magnetic axis for sub-sonic poloidal flow while it is broader for super-sonic poloidal flow compared with that for the static equilibrium. These transitions of the effects of toroidal and poloidal curvatures result in the transitions in the poloidal profiles and the flux average of the pressure, respectively. We have also obtained the analytic representation of the flux coordinates by the expansion of the geometric coordinates with respect to the inverse aspect ratio. The flux coordinates will be applied to the stability analysis of equilibrium with flow.

[1] Hazeltine R D and Meiss J D 1992 *Plasma Confinement* (Redwood City: Addison Wesley)
[2] Goedbloed J P, Keppens R and Poedts S 2010 *Advanced Magnetohydrodynamics* (Cambridge: Cambridge University Press)
[3] Dewar R L, Grimm R C, Johnson J L, Frieman E A, Greene J M and Rutherford P H 1974 *Phys. Fluids* **17** 930
[4] Kleibergen R and Goedbloed J P 1988 *Plasma Phys. Control. Fusion* **30** 1939
[5] Haas F A 1972 *Phys. Fluids* **15** 141
[6] Freidberg J P 1987 *Ideal Magnetohydrodynamics* (New York: Plenum Press)
[7] Zehrfeld H P and Green B J 1972 *Nucl. Fusion* **12** 569
[8] Hameiri E 1983 *Phys. Fluids* **26** 230
[9] Maschke E K and Perrin H 1980 *Plasma Phys.* **22** 579
[10] Shaing K C, Hazeltine R D and Sanuki H 1992 *Phys. Fluids B* **4** 404
[11] Betti R and Freidberg J P 2000 *Phys. Plasmas* **7** 2439
[12] Zelazny R, Stankiewicz R, Galkowski A and Potempski S 1993 *Plasma Phys. Control. Fusion* **35** 1215
[13] Beliën A J C, Botchev M A, Goedbloed J P, van der Holst B and Keppens R 2002 *J. Comp. Phys.* **182** 91
[14] Guazzotto L, Betti R, Manickam J and Kaye S 2004 *Phys. Plasmas* **11** 604
[15] Guazzotto L and Betti R 2005 *Phys. Plasmas* **12** 056107
[16] Ito A, Ramos J J and Nakajima N 2008 *Plasma Fusion Res.* **3** 034
[17] Ito A and Nakajima N 2008 *AIP Conf. Proc* **1069** 121
[18] Raburn D and Fukuyama A 2010 *Phys. Plasmas* **17** 122504
[19] Ito A and Nakajima N 2011 *Nucl. Fusion* **51** 123006
[20] Ito A and Nakajima N 2009 *Plasma Phys. Control. Fusion* **51** 035007
[21] Ito A and Nakajima N 2019 *Plasma Phys. Control. Fusion* **61** 029501
[22] Ito A and Nakajima N 2013 *J. Phys. Soc. Japan* **82** 064502
[23] Kuiroukidis A and Throumoulopoulos G N 2014 *Plasma Phys. Control. Fusion* **56** 075003
[24] López O E and Guazzotto L 2017 *Phys. Plasmas* **24** 032501
[25] Bondeson A, Iacono R, and Bhattacharjee A 1987 *Phys. Fluids* **30** 2167
[26] Frieman E and Rotenberg M 1960 *Rev. Mod. Phys.* **32** 898
[27] Strauss H R 1983 *Nucl. Fusion* **23** 649
[28] Ito A and Nakajima N 2010 *Proc. 23rd IAEA Fusion Energy Conference* THC/P5-03
[29] Bender C M and Orszag S A 1978 *Advanced Mathematical Methods for Scientists and Engineers* (New York: McGraw-Hill) Chap.7
[30] Yamazaki K and Uchida T 1979 *Japan. J. Appl. Phys.* **18** 981
[31] Ito A, Ramos J J and Nakajima N 2007 *Phys. Plasmas* **14** 062502
[32] Jardin S 2010 *Computational Methods in Plasma Physics* (Boca Raton: CRC Press)

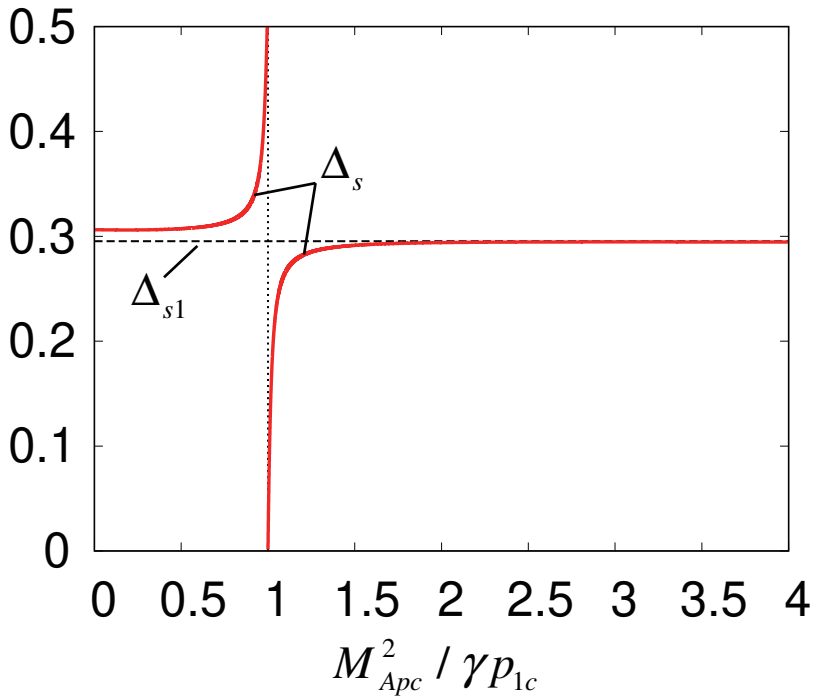


**Figure 1.** Shift of the magnetic axis $\Delta_s$ as a function of the square of the poloidal Mach number $M^2_{Apc}/\gamma p_{1c}$.

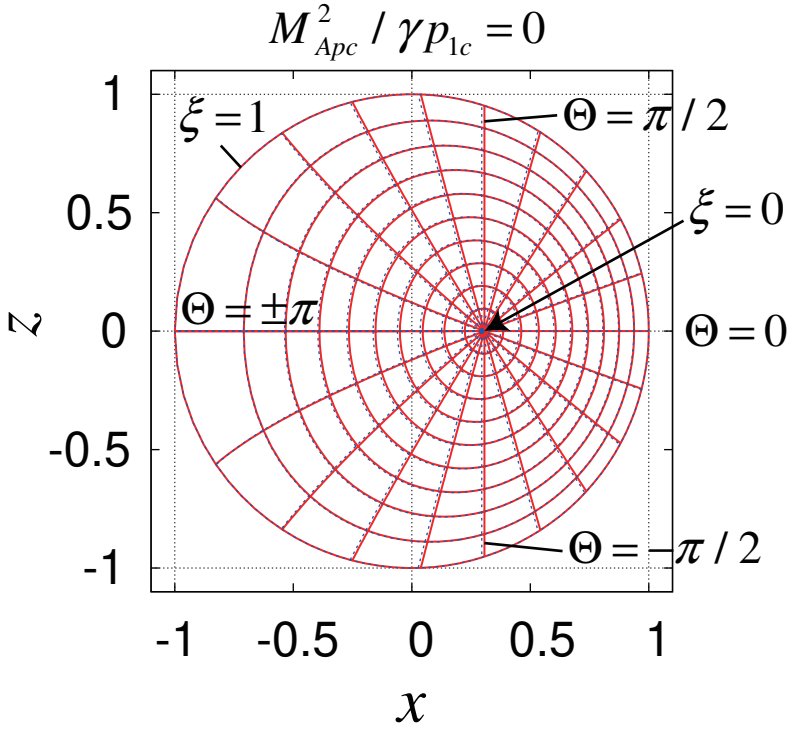


**Figure 2.** Flux coordinates $(\xi, \Theta)$ obtained from $\psi \simeq \psi_1 + \varepsilon\psi_2$ for $M^2_{Apc}/\gamma p_{1c} = 0$ (solid lines) and from $\psi_1$ (dotted lines) in the poloidal cross section.

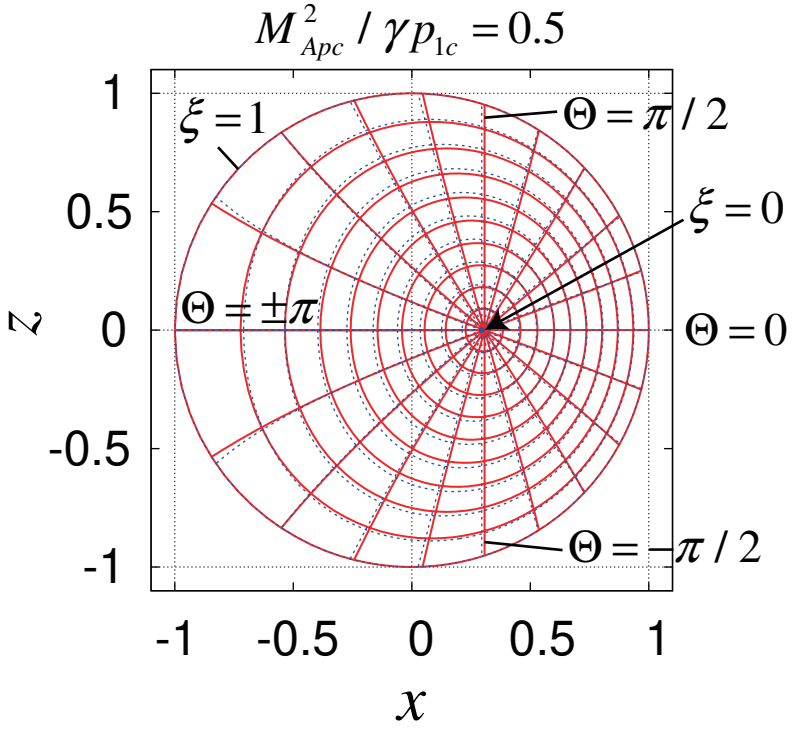


**Figure 3.** Flux coordinates $(\xi, \Theta)$ obtained from $\psi \simeq \psi_1 + \varepsilon\psi_2$ for $M^2_{Apc}/\gamma p_{1c} = 0.5$ (solid lines) and from $\psi_1$ (dotted lines) in the poloidal cross section.

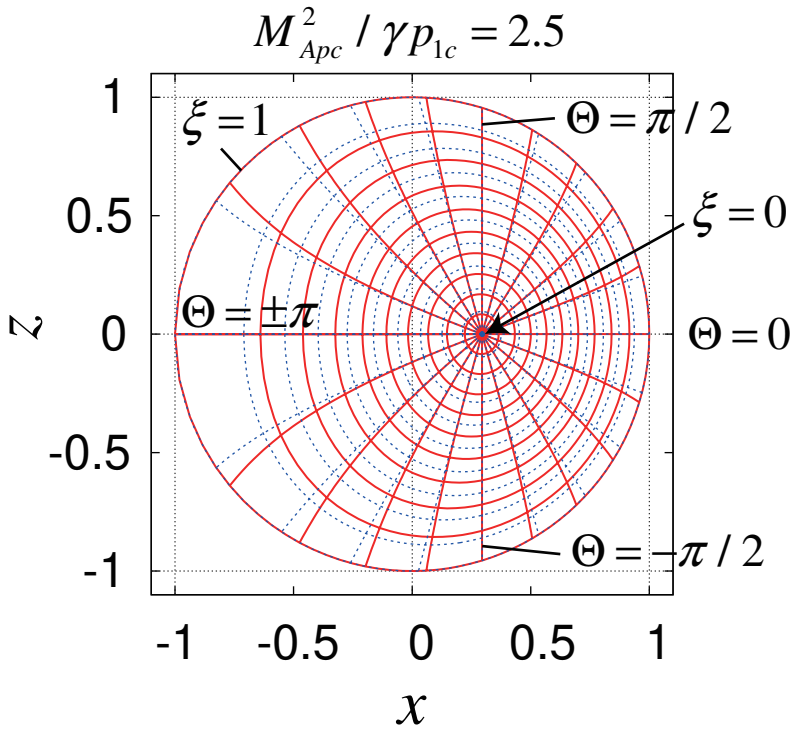


**Figure 4.** Flux coordinates $(\xi, \Theta)$ obtained from $\psi \simeq \psi_1 + \varepsilon\psi_2$ for $M^2_{Apc}/\gamma p_{1c} = 2.5$ (solid lines) and from $\psi_1$ (dotted lines) in the poloidal cross section.

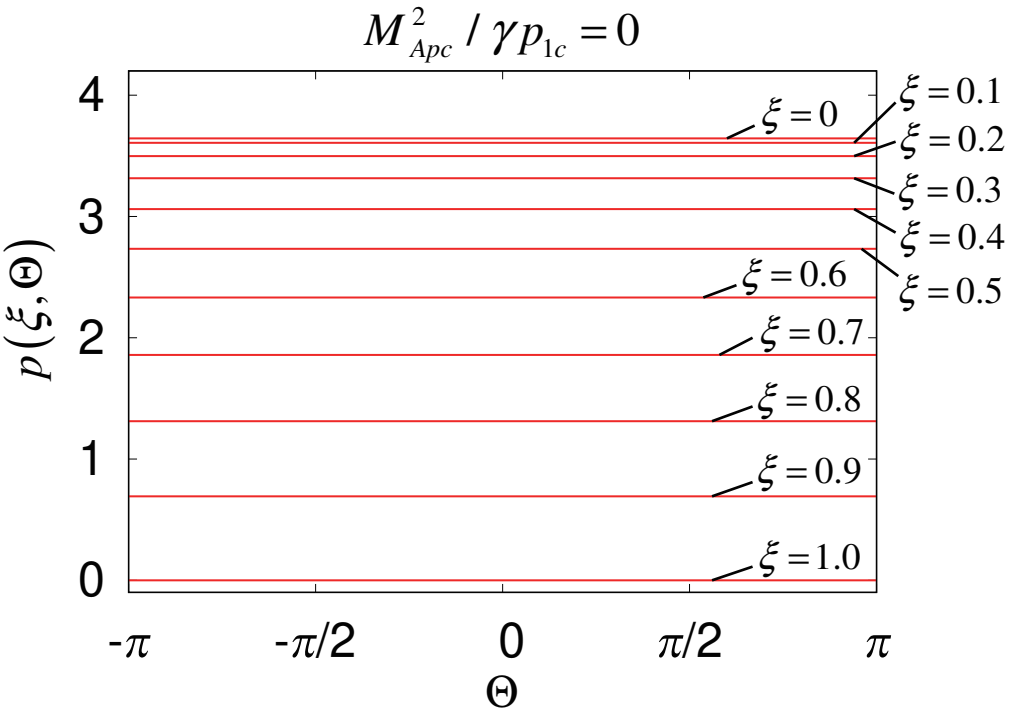


**Figure 5.** Poloidal profiles of the pressure on each flux surface for $M^2_{Apc}/\gamma p_{1c} = 0$.

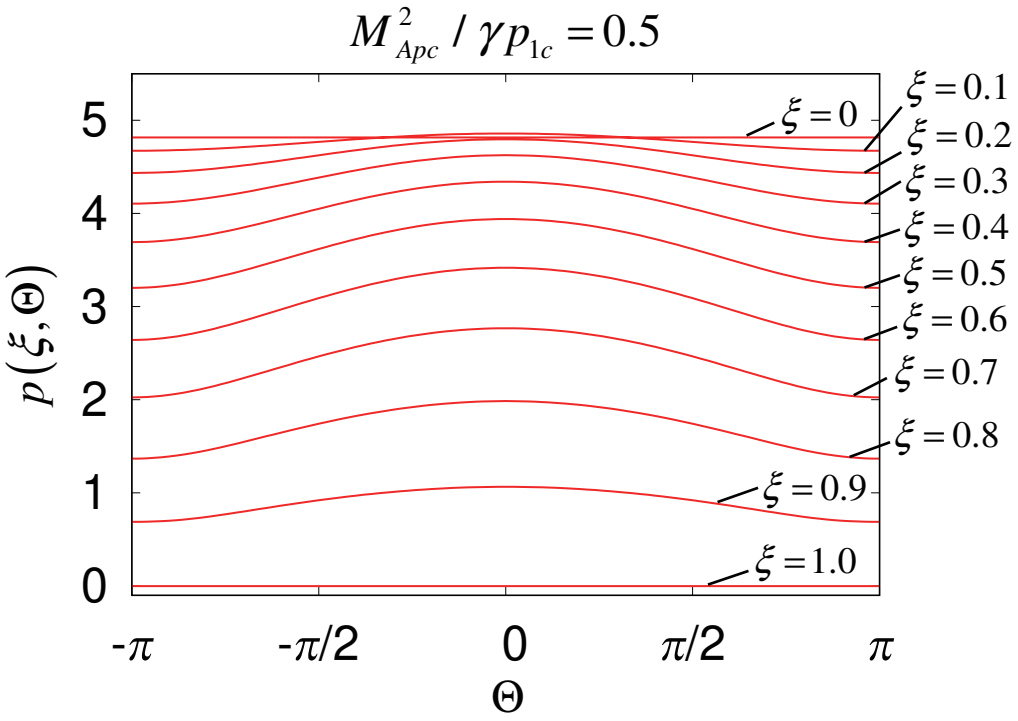


**Figure 6.** Poloidal profiles of the pressure on each flux surface for $M^2_{Apc}/\gamma p_{1c} = 0.5$.

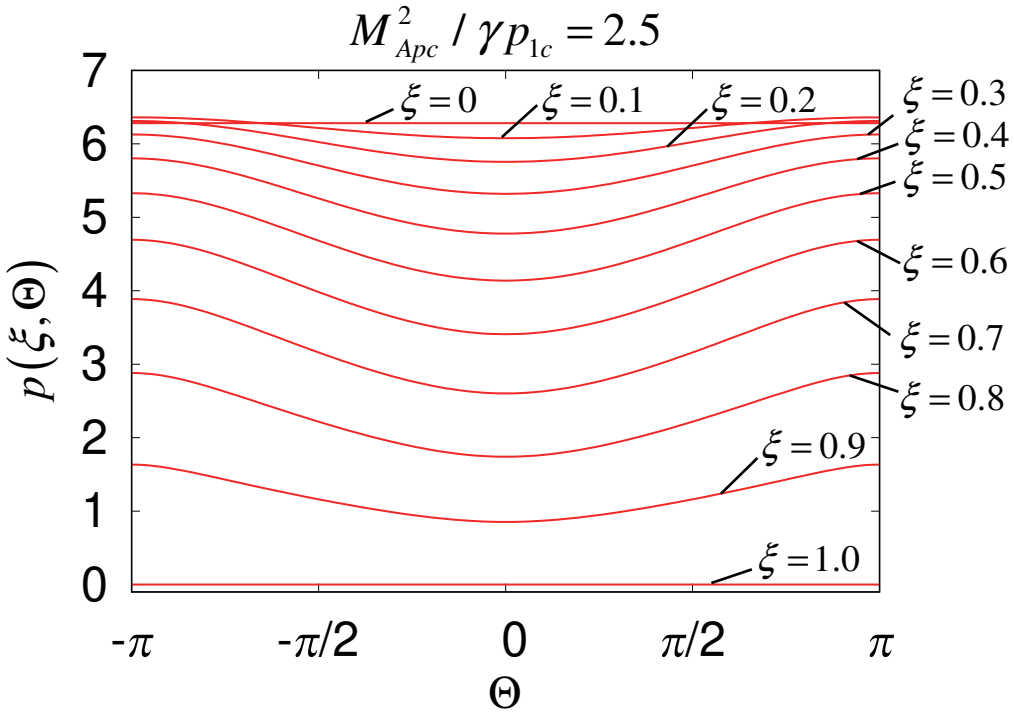


**Figure 7.** Poloidal profiles of the pressure on each flux surface for $M^2_{Apc}/\gamma p_{1c} = 2.5$.

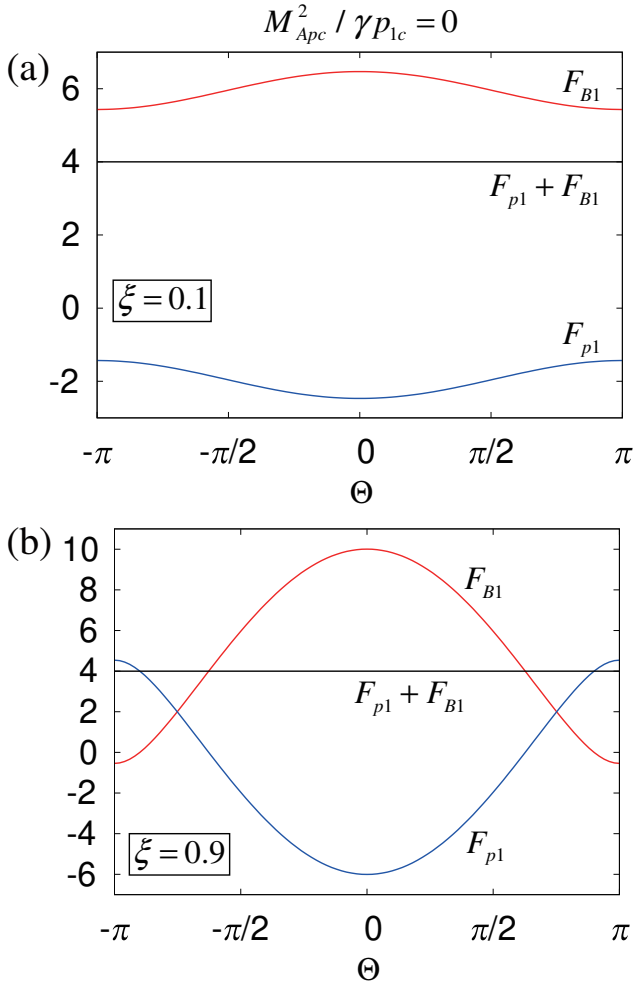


**Figure 8.** First order force balance at different flux surfaces for the static equilibrium, $M^2_{Apc}/\gamma p_{1c} = 0$.

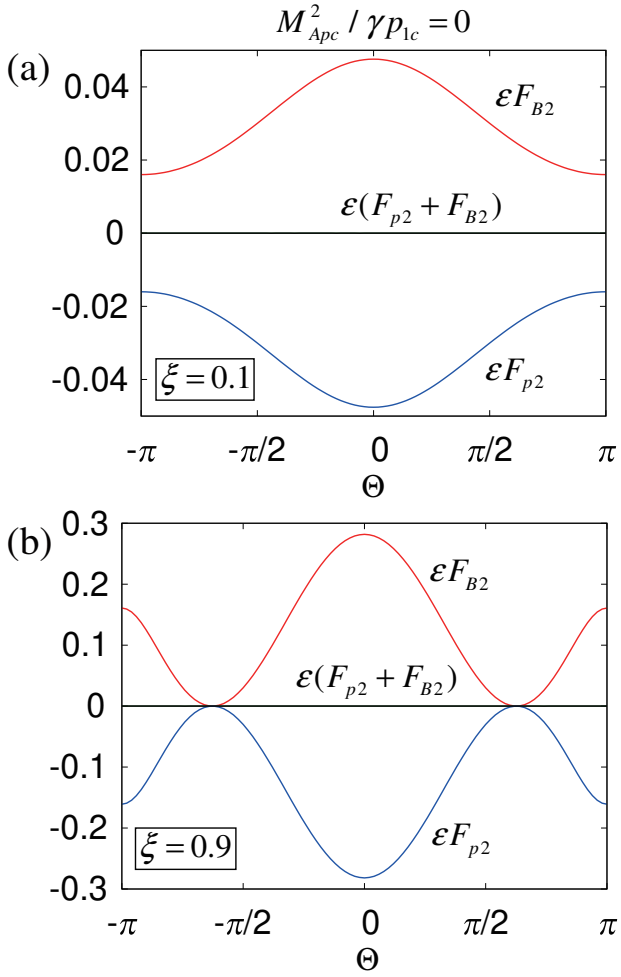


**Figure 9.** Second order force balance for the static equilibrium, $M^2_{Apc}/\gamma p_{1c} = 0$.

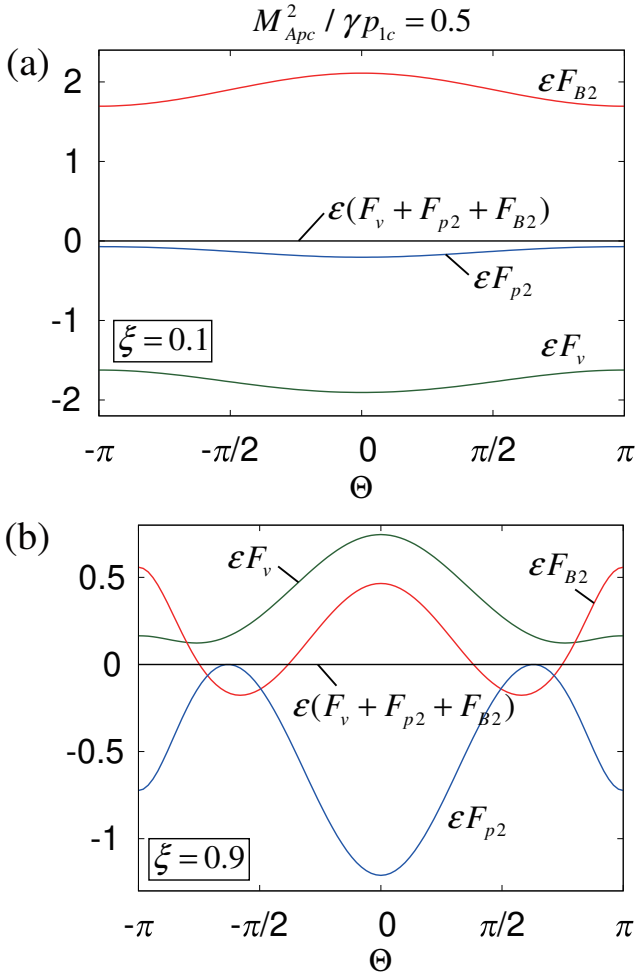


**Figure 10.** Second order force balance for the equilibrium with sub-sonic flow, $M^2_{Apc}/\gamma p_{1c} = 0.5$.

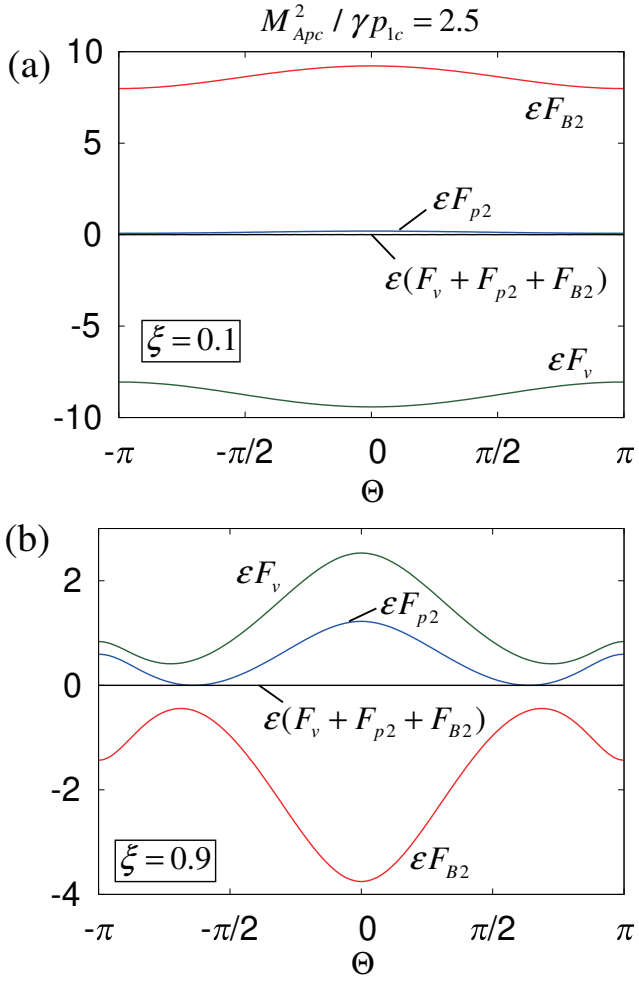


**Figure 11.** Second order force balance for the equilibrium with super-sonic flow, $M^2_{Apc}/\gamma p_{1c} = 2.5$.

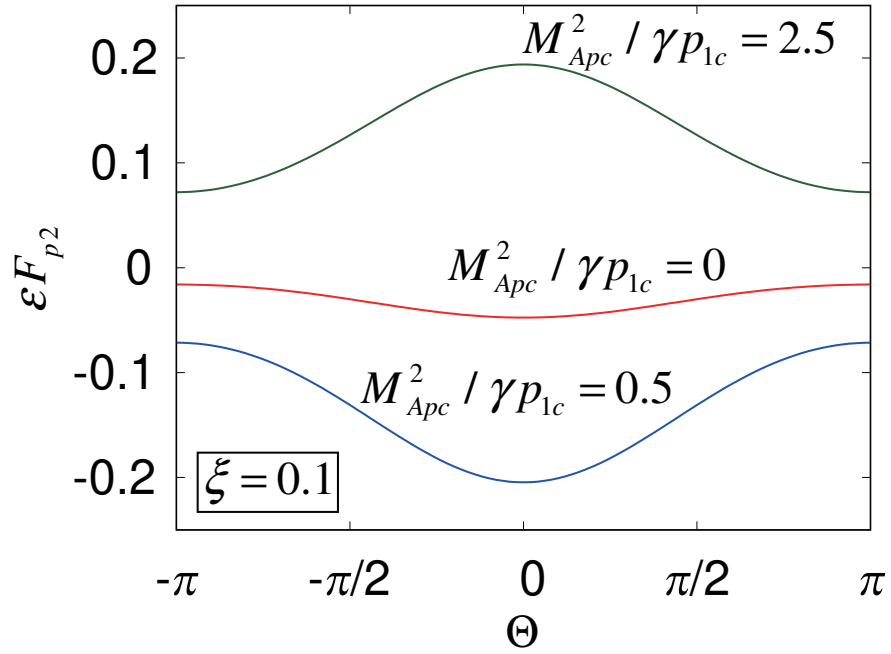


**Figure 12.** Second order pressure forces for different poloidal Mach numbers $M^2_{Apc}/\gamma p_{1c} = 0$, 0.5, and 2.5 at $\xi = 0.1$.

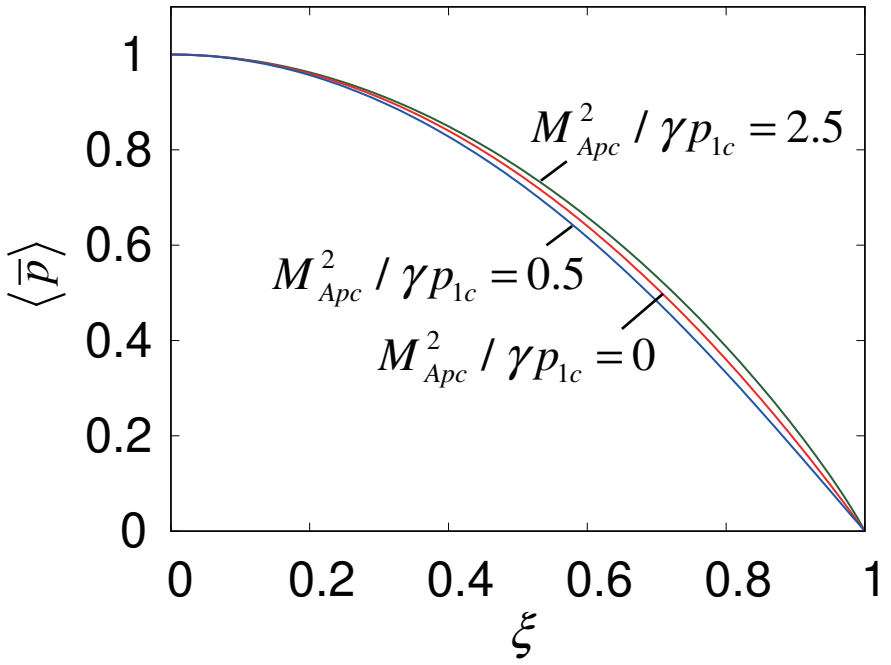


**Figure 13.** Profiles in $\xi$ of the flux surface average of the pressure for different values of the square of the poloidal Mach number $M^2_{Apc}/\gamma p_{1c}$.

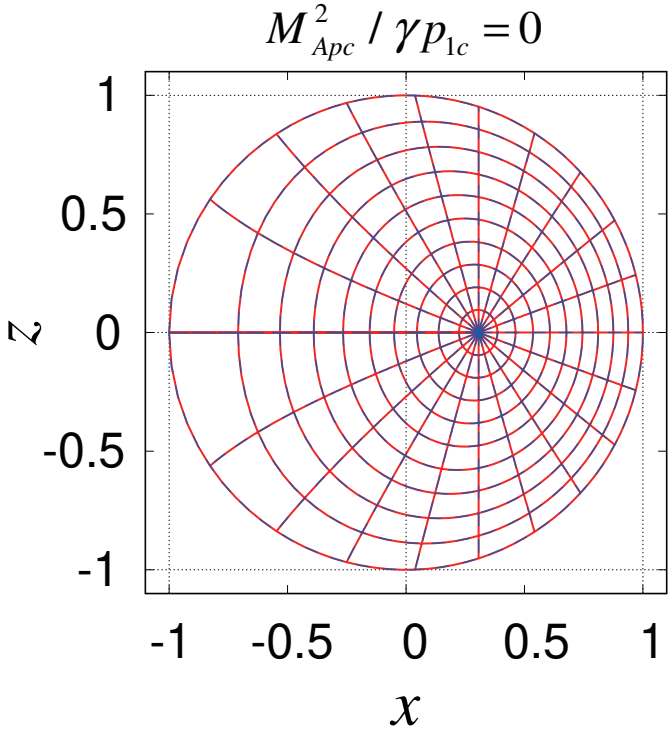


**Figure 14.** Flux coordinate systems $(\xi, \Theta)$ of analytic solution, (88) and (89) (solid lines) and of the numerical solution of (71) and (72) (dashed lines) for $M^2_{Apc}/\gamma p_{1c} = 0$ in the poloidal cross section.

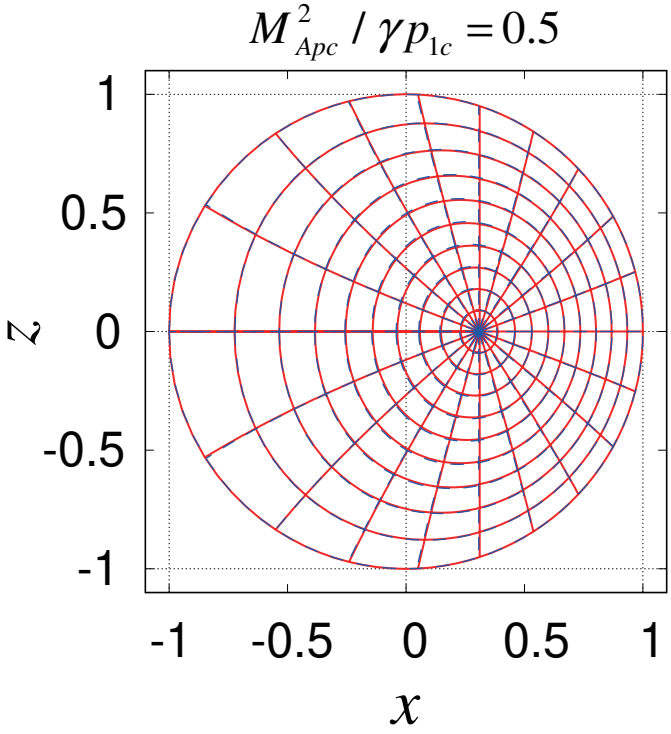


**Figure 15.** Flux coordinate systems $(\xi, \Theta)$ of analytic solution, (88) and (89) (solid lines) and of the numerical solution of (71) and (72) (dashed lines) for $M^2_{Apc}/\gamma p_{1c} = 0.5$ in the poloidal cross section.

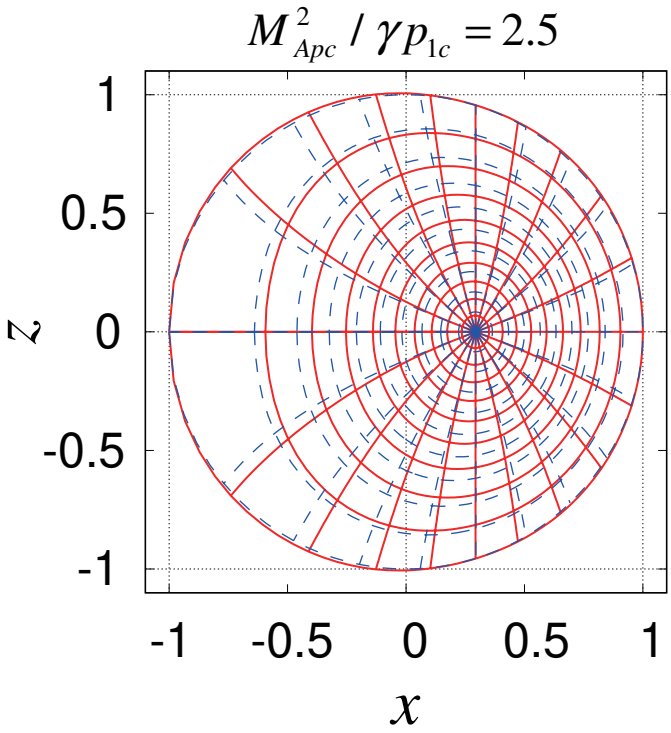


**Figure 16.** Flux coordinate systems $(\xi, \Theta)$ of analytic solution, (88) and (89) (solid lines) and of the numerical solution of (71) and (72) (dashed lines) for $M^2_{Apc}/\gamma p_{1c} = 2.5$ in the poloidal cross section.